Eur. J. Mineral.
2007, **19**, 267–279

# Lead-antimony sulfosalts from Tuscany (Italy). IX. Marrucciite, $Hg_3Pb_{16}Sb_{18}S_{46}$, a new sulfosalt from Buca della Vena mine, Apuan Alps: Definition and crystal structure

PAOLO ORLANDI[1,*], YVES MOËLO[2], ITALO CAMPOSTRINI[3] and ALAIN MEERSCHAUT[2]

[1] Dipartimento di Scienze della Terra, Università di Pisa, Via S. Maria 53, 56126 Pisa, Italy
*Corresponding authors, e-mail: orlandi@dst.unipi.it, Yves.Moelo@cnrs-imn.fr
[2] Institut des Matériaux Jean Rouxel, UMR 6502 CNRS-Université de Nantes, Laboratoire de Chimie des Solides, 2, rue de la Houssinière, 44 322 Nantes Cedex 3, France
[3] Dipartimento di Chimica Strutturale e Stereochimica Inorganica, Via Venezian 21, 20133 Milano, Italia

**Abstract:** Marrucciite, $Hg_3Pb_{16}Sb_{18}S_{46}$, is a new sulfosalt discovered in the Fe-Ba deposit of Buca della Vena, Apuan Alps (Italy). It occurs as black acicular metallic crystals in calcite veins; reflectance values in air are (R %, λ nm): 33.1 (*470*), 30.0 (*546*), 28.8 (*589*), 26.5 (*650*). Marrucciite is monoclinic, space group *C*2/*m*, with *a* 48.32(1) Å, *b* 4.117(1) Å, *c* 24.056(5) Å, β 118.84(3)°, *V* 4192(3) Å$^3$, Z = 2, $D_{calc.}$ = 6.00 g/cm$^3$; a 2*b* superstructure is present. Main lines of the X-ray diffraction powder pattern [d (in Å), *I* (main hkl)]: 4.02, *33* ($\overline{12}$.0.3, 802); 3.480, *64* (803, 604); 3.418, *88* ($\bar{6}$07, 10.0.2, $\bar{3}$14) ; 3.106, *31* ($\bar{9}$.1.4); 2.994, *100* ($\overline{11}$.1.2); 2.922, *41* ($\overline{11}$.1.1); 2.056, *52* (020); 1.764, *41* ($\bar{6}$27). Electron microprobe analysis gave (wt.%; mean of 4 spot analyses): Cu 0.18(12), Hg 7.90(9), Pb 42.41(7), Sb 29.71(7), S 19.47(18), Cl 0.06(2), sum 99.73(14). The chemical formula (basis: 46 (S + Cl) at.) is $Cu_{0.21}Hg_{2.98}Pb_{15.46}Sb_{18.44}S_{45.87}Cl_{0.13}$, giving the stoichiometric one $Hg_3Pb_{16}Sb_{18}S_{46}$ that fulfils the charge balance. X-ray single crystal study (R = 9.56 %) revealed a complex structure, with Hg in two specific distorted octahedral coordinations (2 short distances each, close to 2.36 Å). There are 40 other independent positions: 7 Pb, 2 (Pb,Sb), 8 Sb and 23 S. The general architecture of the structure is strongly related to that of hexagonal $Ba_{12}Bi_{24}S_{48}$, with three types of $Me_{10}S_{14}$ rods (× 2) around a $HgSb_2Pb_4S_4$ central column. It explains the pseudo-hexagonal symmetry (*a*/2 ~ *c*; β ~ 120°). A strong topologic relationship exists also between marrucciite and scainiite. Like rouxelite, the other coexisting Hg bearing sulfosalt, marrucciite was formed by hydrothermal process during the Apenninic tectono-metamorphic event.

**Key-words:** marrucciite, new mineral, sulfosalt, lead, antimony, mercury, crystal structure, Tuscany, Italy.

**Résumé:** La marrucciite, $Hg_3Pb_{16}Sb_{18}S_{46}$, est un nouveau sulfosel découvert dans le gisement à Fe-Ba de Buca della Vena (Alpes Apuanes, Italie). Elle se présente en cristaux aciculaires noirs à éclat métallique dans des veines de calcite. Réflectance dans l'air (R %, λ nm): 33,1 (*470*), 30,0 (*546*), 28,8 (*589*), 26,5 (*650*). La marrucciite est monoclinique, de groupe d'espace *C*2/*m*, avec *a* 48,32(1) Å, *b* 4,117(1) Å, *c* 24,056(5) Å, β 118,84(3)°, *V* 4192(3) Å$^3$, Z = 2, $D_{calc.}$ = 6,00 g/cm$^3$; une surstructure doublant *b* est observable. Les principales raies de diffraction du diagramme de poudre aux rayons X sont [d (Å), *I* (indices hkl)]: 4,02, *33* ($\overline{12}$.0.3, 802); 3,480, *64* (803, 604); 3,418, *88* ($\bar{6}$07, 10.0.2, $\bar{3}$14); 3,106, *31* ($\bar{9}$.1.4); 2,994, *100* ($\overline{11}$.1.2); 2,922, *41* ($\overline{11}$.1.1); 2,056, *52* (020); 1,764, *41* ($\bar{6}$27). L'analyse à la microsonde électronique donne (poids %; moyenne de 4 analyses): Cu 0,18(12), Hg 7,90(9), Pb 42,41(7), Sb 29,71(7), S 19,47(18), Cl 0,06(2), total 99,73(14). La formule chimique, sur la base d'un total de 46 atomes de S et Cl, est $Cu_{0,21}Hg_{2,98}Pb_{15,46}Sb_{18,44}S_{45,87}Cl_{0,13}$, conduisant à la formule stœchiométrique équilibrée $Hg_3Pb_{16}Sb_{18}S_{46}$. L'étude structurale aux rayons X sur monocristal (R = 9,56 %) révèle une structure complexe, avec Hg dans deux sites spécifiques octaédriques aplatis (2 distances courtes Hg-S à 2,36 Å). Il y a 40 autres positions indépendantes: 7 Pb, 2 (Pb,Sb), 8 Sb et 23 S. L'architecture générale de la structure est très semblable à celle de $Ba_{12}Bi_{24}S_{48}$ hexagonal, avec trois types de baguettes $Me_{10}S_{14}$ (× 2) autour d'une colonne centrale $HgSb_2Pb_4S_4$. Ceci explique la symétrie pseudo hexagonale (*a*/2 ~ *c*; β ~ 120°). Une forte similitude topologique existe également entre les structures de la marrucciite et de la scainiite. Tout comme l'autre sulfosel mercurifère associé, la rouxélite, la marrucciite s'est formée par voie hydrothermale durant la phase tectono-métamorphique apennine.

## Introduction

Buca della Vena mine is a small Fe-Ba deposit in the southern part of Apuan Alps, near Pietrasanta, Tuscany (Benvenuti *et al.*, 1986), which presents a complex mineralogy (Orlandi & Checchi, 1986; Orlandi & Dini, 2004). Many lead-antimony sulfosalts are present, and four new ones have been recently defined: scainiite, pillaite, pellouxite and

0935-1221/07/0019-1718 $ 5.85
DOI: 10.1127/0935-1221/2007/0019-1718

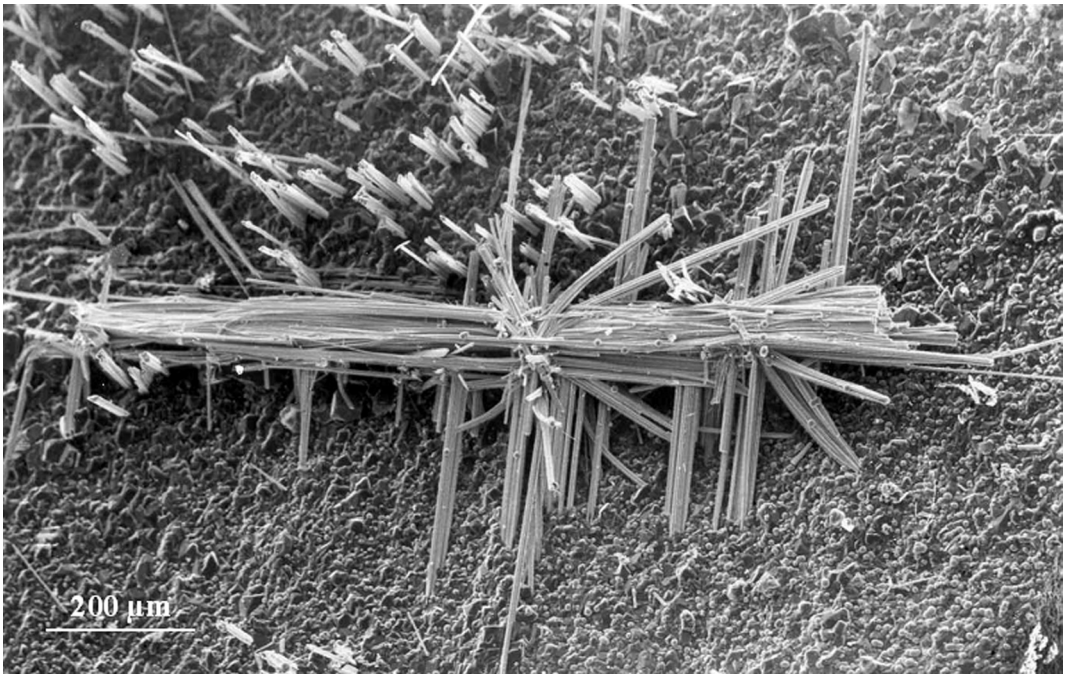


Fig. 1. SEM image of marrucciite fibres and laths. The longest crystals are about 2 mm.

rouxelite (Orlandi *et al.*, 1999; 2001; 2004; 2005). The present study deals with a fifth new sulfosalt of this type, marrucciite, $Hg_3Pb_{16}Sb_{18}S_{46}$.

This new mineral and its name have been approved by the CNMMN of the IMA (No 2006–015). The name is in honour of Angelo Marrucci (1956–2003), a very careful mineral collector, for his contributions to the mineralogy of Tuscany. Type material of marrucciite is deposited at Museo di Storia Naturale e del Territorio, University of Pisa (Italy).

During the study of marrucciite, Ernst Burke, chairman of the CNMMN of the IMA, reported to us the description of the same mineral in another occurrence, the Gelnica (Slovakia) deposit (Háber *et al.*, 2004). These authors named the mineral 'gelnicaite', but without having submitted any official proposal to the CNMMN; moreover, a wrong unit cell was given (see below). A comment by Ernst Burke on this question is given as an addendum at the end of this paper.

## Mineralogical characterization

### Appearance and physical properties

At Buca della Vena, marrucciite was formed together with other lead sulfosalts in the latest hydrothermal stage, within small veinlets crosscutting dolomitic lenses interstratified in the Ba-Fe ore. Like rouxelite, the other Hg bearing sulfosalt from Buca della Vena, marrucciite is extremely rare. It occurs as black acicular crystals with metallic lustre, elongated and striated or bundled parallely to [010] (Fig. 1). Hardness could not be determined due to the small size and scarcity of the crystals. Under the binocular, small fibres are elastic, and may be easily split due to a perfect cleavage parallel to the elongation. According to the crystal structure (see below), the cleavage plane would be $(20\bar{1})$.

In reflected light, marrucciite is light grey, with weak bireflectance, without pleochroism. Euhedral fibres in dolomite or quartz may present a lozenge section. Between crossed polars, the anisotropy is distinct for sub-longitudinal sections, without marked polarisation tints (dark blue to dark brown), and very weak for sub-perpendicular ones. Red internal reflections are sometimes visible for thinnest fibres or at the contact with gangue minerals. No twinning was observed. Marrucciite is thus difficult to be distinguished from more common Pb-Sb sulfosalts like boulangerite or robinsonite.

Reflectance data in air on a random section are given in Table 1. The reflectance curve (Fig. 2) decreases regularly,

Table 1. Marrucciite: reflectance data (random section) from 400 to 800 nm in air.

| λ (nm) | $R_{air}$ | λ (nm) | $R_{air}$ | λ (nm) | $R_{air}$ | λ (nm) | $R_{air}$ |
|---|---|---|---|---|---|---|---|
| 400 | (33.0)* | 500 | 32.0 | 600 | 27.1 | 700 | 25.5 |
| 410 | 37.2 | 510 | 31.1 | 610 | 27.1 | 710 | 25.4 |
| 420 | 36.7 | 520 | 30.6 | 620 | 28.2 | 720 | 25.8 |
| 430 | 35.4 | 530 | 29.9 | 630 | 26.1 | 730 | 23.2 |
| 440 | 35.0 | 540 | 30.1 | 640 | 27.1 | 740 | 25.3 |
| 450 | 34.6 | 550 | 29.8 | 650 | 26.5 | 750 | 23.3 |
| 460 | 33.4 | 560 | 29.7 | 660 | 26.7 | 760 | 24.0 |
| 470 | 33.1 | 570 | 28.2 | 670 | 26.4 | 770 | 22.1 |
| 480 | 32.5 | 580 | 28.5 | 680 | 26.1 | 780 | 21.8 |
| 490 | 31.9 | 590 | 28.8 | 690 | 26.2 | 790 | 22.8 |
| | | | | | | 800 | 22.8 |
| 470 | 33.1 | 546 | 30.0 | 589 | 28.8 | 650 | 26.5 |

Polishing method: 6, 1 , ¼ and $^1/_{10}$ diamond on cloth; final buffing with $Cr_2O_3$ on cloth. LEICA DMR microscope with objective FLUOTAR 20×/0.50 POL. Microscope photometer: Leica MPV-SP, monochromator: Δλ = 2 nm. Standard: SiC (NPL n°50). *: too low value.

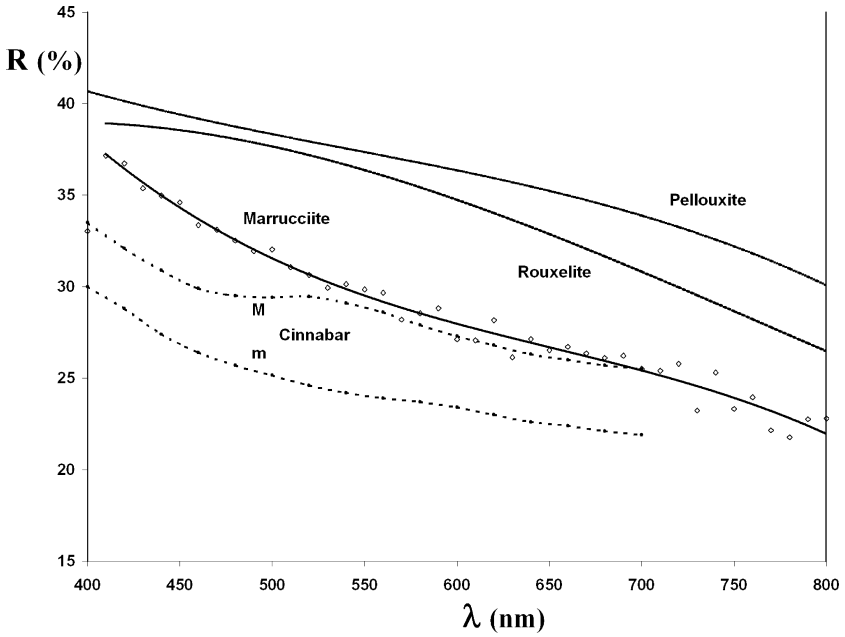


Fig. 2. Reflectance curve in air for a random section of marrucciite, compared with those of pellouxite (Orlandi *et al.*, 2004), rouxelite (Orlandi *et al.*, 2005) and cinnabar (Criddle & Stanley, 1993; M and m: maximal and minimal values).

Table 2. Electron-probe microanalysis of marrucciite from Buca della Vena (this study) and Zenderling (Haber *et al.*, 2004).

| a) weight % | | | | | | | | |
|---|---|---|---|---|---|---|---|---|
| Buca della Vena | | | | | | | | |
| | Anal. No | Cu | Hg | Pb | Sb | S | Cl | Total |
| Sample A | 1 | 0.14 | 7.53 | 41.98 | 28.98 | 19.02 | 0.06 | 97.71 |
| | 2 | 0.21 | 7.70 | 42.25 | 29.22 | 19.33 | 0.15 | 98.86 |
| | 3 | 0.27 | 8.29 | 42.06 | 28.79 | 18.85 | 0.00 | 98.26 |
| | 4 | 0 | 7.77 | 42.37 | 28.95 | 18.97 | 0.04 | 98.10 |
| | 5 | 0 | 7.25 | 42.32 | 28.92 | 18.76 | 0.04 | 97.29 |
| | 6 | 0 | 7.61 | 42.25 | 28.81 | 19.13 | 0.06 | 97.86 |
| | 7 | 0 | 7.97 | 41.99 | 29.07 | 18.97 | 0.05 | 98.05 |
| | Mean | 0.09 | 7.73 | 42.17 | 28.96 | 19.00 | 0.06 | 98.02* |
| | σ | 0.12 | 0.33 | 0.16 | 0.15 | 0.19 | 0.05 | 0.49 |
| Sample B | 8 | 0.10 | 7.98 | 42.38 | 29.79 | 19.22 | 0.06 | 99.53 |
| | 9 | 0.19 | 7.78 | 42.51 | 29.66 | 19.54 | 0.06 | 99.74 |
| | 10 | 0.34 | 7.90 | 42.41 | 29.65 | 19.49 | 0.04 | 99.83 |
| | 11 | 0.08 | 7.94 | 42.34 | 29.75 | 19.64 | 0.08 | 99.83 |
| | Mean | 0.18 | 7.90 | 42.41 | 29.71 | 19.47 | 0.06 | 99.73 |
| | σ | 0.12 | 0.09 | 0.07 | 0.07 | 0.18 | 0.02 | 0.14 |
| Struc.** | | | 7.93 | 43.87 | 28.76 | 19.44 | | 100 |
| Zenderling (Haber *et al.*, 2004) | | | | | | | | |
| | min. | 0.00 | 7.71 | 42.25 | 29.25 | 19.64 | | 99.98*** |
| | max | 0.03 | 8.30 | 42.97 | 30.16 | 19.93 | | 100.41*** |
| Ideal – $Hg_3Pb_{16}Sb_{18}S_{46}$ (calc.) | | | 7.94 | 43.71 | 28.90 | 19.45 | | 100 |

Detection limit (wt.%): Cu 0.08; Cl 0.03. * Low total due to fine-grained sample.
** According to the formula given by the crystal structure study, $Hg_3Pb_{16.07}Sb_{17.93}S_{46}$.
*** Additional minor chemical elements (wt.%): Bi (0.02–0.33); Zn (0.02–0.06).

as it is generally the case for lead-antimony sulfosalts (Criddle & Stanley, 1993). For comparison are given the reflectance curves for pellouxite (with close Pb/Sb ratio, and without Hg), rouxelite (with lower Hg content), and cinnabar HgS. It appears that an increasing Hg content induces a general decrease of the reflectance, especially for the high wavelengths. It may correspond to a shift of the absorption band towards the short wavelengths, that is an opening of the band gap.

Density could not be measured due to the paucity of this sulfosalt. According to the empirical formula resulting from

EPMA (sample A), $D_{calc.} = 6.010$ g/cm$^3$, against 6.004 g/cm$^3$ for the stoichiometric one, $Hg_3Pb_{16}Sb_{18}S_{46}$.

## Chemistry

Qualitative SEM-EDS chemical analysis of marrucciite showed major lead, antimony, mercury and sulphur. Electron probe microanalysis (EPMA) was performed on a Cameca SX 50 apparatus (common laboratory BRGM-CNRS-University at Orléans, France). Operating conditions were as follows: 20 kV (10 kV for oxygen), 20 nA, standards [element (*emission line*, counting time for one spot analysis)]: PbS (Pb *M*α, 20 s), pyrite (S*K*α, 10 s), stibnite (Sb *L*α, 10 s), HgS (Hg *M*α, 20 s), Cu metal (Cu*K*α, 10 s), pyromorphite (Cl*K*α, 10 s).

Analytical results obtained on two distinct samples A and B are presented in Table 2. Contrary to other new lead sulfosalts defined at Buca della Vena (see references above), no oxygen was detected, which was confirmed by the crystal structure study. Traces of Cu (up to 0.34 wt.%) and Cl (up to 0.15 wt.%) are present.

On the basis of S + Cl = 46 apfu, the empirical formula given by EPMA for samples A and B are $Cu_{0.11}Hg_{2.98}Pb_{15.76}Sb_{18.41}S_{45.88}Cl_{0.11}$ and $Cu_{0.21}Hg_{2.98}Pb_{15.46}Sb_{18.44}S_{45.87}Cl_{0.13}$, respectively, in accordance with the formula given by the crystal structure study, $Hg_3Pb_{16.07}Sb_{17.93}S_{46}$ (see below). The proposed stoichiometric formula, fulfilling the valence equilibrium, is $Hg_3Pb_{16}Sb_{18}S_{46}$.

The sulfosalt described by Háber & Babčan (1971) and Háber *et al.* (2004) at Zenderling near Gelnica (Slovakia) was given ideally as $5PbS.HgS._3Sb_2S_3$, which is very close to $Hg_3Pb_{16}Sb_{18}S_{46}$. The actual microprobe analysis given by Háber *et al.* (2004) (Table 2) fully agrees with that of marrucciite from Buca della Vena.

## X-ray data

Rotation, Weissenberg, precession and Gandolfi photographs permitted to select single crystals of marrucciite, but only registration with a Brucker-Nonius diffractometer permitted to determine the unit cell data on two single crystals. Marrucciite is monoclinic, space group *C*2/*m*, with *a* 48.32(1) Å, *b* 4.117(1) Å, *c* 24.056(5) Å, β 118.84(3)°, *V* 4192(3) Å$^3$, Z = 2. According to Bragg photographs, there is a 2*b* superstructure, confirmed by rare weak reflections visible on CCD images. The X-ray powder-diffraction pattern has been obtained with a Gandolfi camera (114.6 mm diameter, with Cu*K*α – see Table 3), and compared with the simulated pattern calculated from the crystal structure (DIAMOND program). Main diffraction lines are [d (in Å), *I* (main hkl)]: 4.02, *33* ($\overline{12}$.0.3, 802); 3.480, *64* (803, 604); 3.418, *88* ($\bar{6}$07, 10.0.2, $\bar{3}$14) ; 3.106, *31* ($\bar{9}$.1.4); 2.994, *100* ($\overline{11}$.1.2); 2.922, *41* ($\overline{11}$.1.1); 2.056, *52* (020); 1.764, *41* ($\bar{6}$27).

Despite a general accordance between measured and calculated diffraction intensities $I_{meas.}$ and $I_{calc.}$, there are some discrepancies (for instance inversion between values of $I_{meas.}$ and $I_{calc.}$ for (hkl) = ($\overline{11}$.1.2) and ($\overline{11}$.1.1) – Table 3), which probably results from different causes: fibrous habit, long-range disorder at the crystal scale, and consequently bad quality of the crystal structure refinement.

Table 2 (cont.)

b) Atom ratio (basis : S + Cl = 46 at.)
Buca della Vena

| | | Cu | Hg | Pb | Sb | S | Cl | Ev* |
|---|---|---|---|---|---|---|---|---|
| Sample A | 1 | 0.17 | 2.90 | 15.67 | 18.41 | 45.87 | 0.13 | 0.71 |
| | 2 | 0.25 | 2.91 | 15.45 | 18.19 | 45.68 | 0.32 | –0.17 |
| | 3 | 0.33 | 3.23 | 15.88 | 18.50 | 46.00 | 0.00 | 2.25 |
| | 4 | 0.00 | 3.01 | 15.87 | 18.45 | 45.91 | 0.09 | 1.30 |
| | 5 | 0.00 | 2.84 | 16.03 | 18.64 | 45.91 | 0.09 | 1.89 |
| | 6 | 0.00 | 2.92 | 15.68 | 18.19 | 45.87 | 0.13 | –0.11 |
| | 7 | 0.00 | 3.08 | 15.72 | 18.52 | 45.89 | 0.11 | 1.38 |
| | Mean | 0.11 | 2.98 | 15.76 | 18.41 | 45.88 | 0.12 | 1.04 |
| | σ | 0.14 | 0.14 | 0.19 | 0.17 | 0.10 | 0.10 | 0.94 |
| Sample B | 8 | 0.12 | 3.04 | 15.65 | 18.72 | 45.87 | 0.13 | 1.98 |
| | 9 | 0.23 | 2.92 | 15.44 | 18.34 | 45.87 | 0.13 | 0.10 |
| | 10 | 0.40 | 2.97 | 15.46 | 18.40 | 45.91 | 0.09 | 0.60 |
| | 11 | 0.09 | 2.96 | 15.29 | 18.28 | 45.83 | 0.17 | –0.41 |
| | Mean | 0.21 | 2.98 | 15.46 | 18.44 | 45.87 | 0.13 | 0.57 |
| | σ | 0.14 | 0.05 | 0.15 | 0.20 | 0.03 | 0.03 | 1.03 |
| Struc. | | | 3 | 16.07 | 17.93 | 46 | | |
| Zenderling | Zn | Cu | Hg | Pb | Sb | S | Bi | |
| Medium composition** | 0.047 | 0.023 | 2.976 | 15.331 | 18.187 | 46 | 0.064 | –0.56 |
| Ideal | | | 3 | 16 | 18 | 46 | | 0 |

* Ev = relative error (%) on the valence equilibrium.
** *i.e.* on the basis of (min. + max.)/2 of Table 1a.

Table 3. X-ray diffraction powder pattern for marrucciite.

| $I_{meas.}$ | $d_{meas.}$ | $d_{calc.}$ | $I_{calc.}$ | h | k | l | $I_{meas.}$ | $d_{meas.}$ | $d_{calc.}$ | $I_{calc.}$ | h | k | l | $I_{meas.}$ | $d_{meas.}$ | $d_{calc.}$ | $I_{calc.}$ | h | k | l |
|---|---|---|---|---|---|---|---|---|---|---|---|---|---|---|---|---|---|---|---|---|
| 7 | 7.7 | 7.90 | 16 | –2 | 0 | 3 | **100** | **2.994** | **2.992** | **44** | **–11** | **1** | **2** | | | 2.1033 | 15 | 15 | 1 | 2 |
| | | 7.88 | 19 | –6 | 0 | 2 | **41** | **2.922** | **2.925** | **100** | **–11** | **1** | **1** | **52** | **2.056** | **2.0585** | **99** | **0** | **2** | **0** |
| 3 | 4.75 | 4.812 | 18 | –10 | 0 | 2 | 20 | 2.850 | 2.863 | 53 | –7 | 1 | 6 | 9 | 2.038 | 2.0372 | 25 | 17 | 1 | 1 |
| | | 4.770 | 20 | –6 | 0 | 5 | | | 2.811 | 51 | 11 | 1 | 0 | 12 | 1.996 | 1.9987 | 14 | –21 | 1 | 4 |
| 3 | 4.57 | 4.578 | 32 | –2 | 0 | 5 | 16 | 2.800 | 2.808 | 25 | –9 | 1 | 6 | 10 | 1.959 | 1.9577 | 10 | 6 | 0 | 9 |
| | | 4.098 | 43 | 1 | 1 | 0 | | | 2.759 | 29 | –13 | 1 | 3 | 3 | 1.936 | 1.9371 | 9 | –6 | 0 | 12 |
| | | 4.058 | 13 | –1 | 1 | 1 | 2 | 2.738 | 2.741 | 7 | –13 | 1 | 3 | 9 | 1.912 | 1.9106 | 32 | –1 | 1 | 10 |
| **33** | **4.02** | **4.026** | **11** | **–12** | **0** | **3** | 2 | 2.722 | 2.721 | 9 | 10 | 0 | 4 | | | 1.8793 | 21 | –21 | 1 | 9 |
| | | **4.015** | **14** | **8** | **0** | **2** | 6 | 2.664 | 2.679 | 30 | –13 | 1 | 5 | 26 | 1.872 | 1.8697 | 18 | –23 | 1 | 6 |
| | | 3.881 | 21 | –1 | 1 | 2 | | | 2.613 | 36 | –9 | 1 | 7 | 30 | 1.838 | 1.8389 | 13 | 17 | 1 | 3 |
| 2 | 3.82 | 3.810 | 14 | 10 | 0 | 1 | 5 | 2.604 | 2.607 | 19 | 1 | 1 | 6 | 17 | 1.775 | 1.7735 | 21 | 8 | 2 | 3 |
| | | 3.733 | 34 | –12 | 0 | 5 | 2 | 2.503 | 2.505 | 14 | 11 | 1 | 2 | **41** | **1.764** | **1.7650** | **18** | **–6** | **2** | **7** |
| 18 | 3.72 | 3.702 | 30 | 5 | 1 | 0 | 3 | 2.488 | 2.491 | 7 | –15 | 1 | 2 | 7 | 1.719 | * | | | | |
| 9 | 3.67 | 3.662 | 20 | –3 | 1 | 3 | 3 | 2.387 | 2.3872 | 13 | –11 | 1 | 8 | 13 | 1.705 | * | | | | |
| | | 3.614 | 14 | –1 | 1 | 3 | 17 | 2.339 | 2.3428 | 34 | –3 | 1 | 8 | 3 | 1.657 | * | | | | |
| | | 3.513 | 22 | –7 | 1 | 1 | | | 2.3252 | 15 | –13 | 1 | 8 | 5 | 1.631 | * | | | | |
| **64** | **3.480** | **3.493** | **62** | **8** | **0** | **3** | | | 2.2790 | 28 | –17 | 1 | 2 | 4 | 1.530 | * | | | | |
| | | **3.490** | **18** | **6** | **0** | **4** | 3 | 2.246 | 2.2416 | 9 | –9 | 1 | 9 | 11 | 1.504 | * | | | | |
| | | 3.446 | 44 | –14 | 0 | 3 | 5 | 2.211 | 2.2147 | 9 | –20 | 0 | 1 | 4 | 1.470 | * | | | | |
| | | 3.433 | 38 | –14 | 0 | 4 | | | 2.1998 | 5 | 8 | 0 | 7 | 5 | 1.459 | * | | | | |
| **88** | **3.418** | **3.430** | **49** | **–6** | **0** | **7** | 6 | 2.199 | 2.1996 | 6 | –5 | 1 | 9 | 7 | 1.413 | * | | | | |
| | | **3.401** | **31** | **10** | **0** | **2** | 4 | 2.186 | 2.1864 | 10 | 9 | 1 | 5 | 15 | 1.365 | 1.3642 | 16 | –31 | 1 | 2 |
| | | **3.389** | **31** | **–3** | **1** | **4** | | | 2.1273 | 28 | –15 | 1 | 9 | 15 | 1.316 | 1.3186 | 17 | –27 | 1 | 16 |
| 9 | 3.251 | 3.261 | 23 | 3 | 1 | 3 | 7 | 2.120 | 2.1264 | 6 | 5 | 1 | 7 | 6 | 1.290 | * | | | | |
| **31** | **3.106** | **3.142** | **40** | **–9** | **1** | **4** | 28 | 2.109 | 2.1072 | 14 | 0 | 0 | 10 | 11 | 1.260 | * | | | | |

* multiple weak lines.

Unit cell data given by Háber *et al.* (2004) for the similar Slovak sulfosalt do not agree with the unit cell of marrucciite. It appears to correspond to the unit cell of associated boulangerite:

- at Zenderling: *a* 4.028, *b* 21.16, *c* 23.47Å, space group *Pmmm*;
- boulangerite with orthorhombic symmetry (Nos are from PCPDFWIN data base): *a* 21.28, *b* 23.52, *c* 4.019 Å, space group *Pbnm* (No 88–2171); *a* 23.49, *b* 21.24, *c* 4.020 Å, space group *Pnam* (No 84–2222); *a* 21.24, *b* 23.51, *c* 4.036 Å, space group *Pbnm* (No 84–0480).

## Crystal structure

### Data collection

Only one needle of marruccite was suitable for an X-Ray single crystal study. This crystal (elongated along *b*) was mounted on a Nonius Kappa CCD diffractometer, using Mo*K*α radiation. Crystal data, data collection and structure refinement are given in Table 4. A total of 25162 reflections was measured to a maximum 2θ of 60.0°, among which 7749 reflections were unique, 9424 weak, and 300 with negative intensities. This data set (22185 reflections read from file "nanny.hkl") was employed for structure solution in the monoclinic symmetry (space group *C*2/*m*), with unit cell parameters as given in 2.3. The rare diffraction spots due to the 2*b* superstructure could not be considered in the data collection.

### Structure determination

The structure of marrucciite was solved by means of direct methods (SHELXS-97) and subsequent difference-Fourier syntheses. Refinement was conducted with the use of the SHELXTL program (XL-crystal structure refinement, version 6.12 Unix, 2001 Bruker-AXS), giving a final R value equal to 0.0956. All final experimental data and refinement results are summarized in Table 4. Table 5 gives atomic coordinates, site occupancy factors (s.o.f.) and equivalent isotropic displacement parameters U(eq/iso), and Table 6 anisotropic displacement parameters for cations.

Figure 3 presents the projection of the unit cell along *b*. There are 23 S positions, among which 7 deviate from $y = 0$ or ½ and have been split "up and down" (with a site occupancy factor (s.o.f.) of 0.5 (Table 5). Among cations, there are 2 Hg positions, 7 pure Pb positions, 8 pure Sb positions, and two Pb/Sb pairs (*i.e.* two distinct positions within the same anionic polyhedron). Among the 8 pure Sb positions, three of them have been split (Nos 1, 7 and 10) with an half occupancy factor.

For the two mixed (Pb,Sb) positions, the Pb/Sb ratios have been refined with a constraint on the site occupancy factors (s.o.f. – see Table 5) such that the resulting number of atoms leads to 4 at., *i.e.* a fully occupied *4i* site. These ratios are close to 0.63(3)/0.37(-) for Pb(8)/Sb(8), and 0.41(3)/0.59(-) for Pb(9)/Sb(9).

The structural formula resulting from this crystal structure study is $Hg_3Pb_{16.07}Sb_{17.93}S_{46}$. According to this, with a total of 46 divalent anions in the structural formula, one

Table 4. Crystal and experimental data, and structure refinement for marrucciite.

| | |
|---|---|
| CRYSTAL DATA | |
| Structural formula | $Hg_3Pb_{16.07}Sb_{17.93}S_{46}$ |
| Formula weight | 7589 g/mol |
| Crystal system | monoclinic |
| Space group | *C2/m* (n°12) |
| *a* | 48.32 (1) Å |
| *b* | 4.1170 (8) Å |
| *c* | 24.056 (5) Å |
| β | 118.84 (3)° |
| V | 4191.9 (14) Å$^3$ |
| Z ; Calculated density | 2 ; 6.013 g/cm$^3$ |
| DATA COLLECTION | |
| Temperature | 293 (2) K |
| Crystal size (mm) | 0.005 × 0.20 × 0.01 |
| Radiation | Mo*K*α (λ = 0.71073 Å) |
| | 60 kV × 27 mA |
| Diffractometer | Nonius Kappa CCD |
| Crystal to detector distance | 34.60 mm |
| θ range | 6.44° to 30.00° |
| Reflections collected | 25162 |
| Unique reflections | 7749 [R-sym = 0.176] |
| Weak reflections | 9424 |
| Negative intensities | 300 |
| Index ranges | $-62 \le h \le 53$ |
| | $-5 \le k \le 5$ |
| | $-31 \le l \le 30$ |
| REFINEMENT | |
| Refinement method | Full-matrix least-squares on F$^2$ |
| $2\theta_{max}$ for refinement | 56° |
| Data/restraints/parameters | 5399/0/204 |
| Goodness-of-fit on F$^2$ | 1.195 |
| R1 [for 3627 refl. with I ≥ 2σ(I)] | 0.0956 |
| R1 index (for all 5399 refl.) | 0.1455 |
| Largest diff. peak/hole (e$^-$.Å$^{-3}$) | 4.19, –3.83 e$^-$.Å$^{-3}$ |

ought to have 16 Pb and 18 Sb atoms besides 3 Hg atoms to respect the valence equilibrium, in agreement with $Hg^{2+}$, $Pb^{2+}$, $Sb^{3+}$ and $S^{2-}$.

## Atom coordination

Mercury atoms: The Hg1 atom presents a classic case of a compressed octahedral coordination (Fig. 4a), with two short opposite bonds with S1 at 2.361 Å (Table 7), and four long equatorial ones with S2 at 3.230 Å. The bond valence sum (BVS), according to Brese & O'Keeffe (1991), is equal to 2.16 valence units (v.u.). For comparison, in cinnabar (trigonal α-HgS), there are two apical bonds at 2.377 Å, and four equatorial ones at 3.093 Å (× 2) and 3.279 Å (× 2).

The Hg2 atom has a more distorted coordination (Fig. 4b), as indicated in Table 7, with BVS = 1.98 v.u. Table 7 gives also S-Hg-S angles, as well as data for Hg in the structure of associated rouxelite for comparison. Data concerning other Hg sulfosalts (livingstonite and grumiplucite) are presented in Orlandi *et al.* (2005).

Lead atoms: All these atoms present a trigonal prismatic coordination, mono- or bicapped. They can also be distinguished depending on whether these prisms are "lying" (*l*) or "standing" (*s*) (prism axis sub-perpendicular or sub-parallel to the *b* axis of projection, respectively). According to Table 8, all monocapped Pb atoms (Nos 2, 3 and 5) are of the "l" type, while the others (Nos 1, 4, 6 and 8) are of the "s" type. Their BVS is close to 2 (from 1.83 up to 2.04).

Antimony atoms: Classically, Sb atoms present a strong bonding with 5 S atoms in a dissymmetric rectangular pyramidal coordination (in order of increasing Sb-S distances: S apex, 2 S at one side of the basal rectangle, 2 opposite S), with one or two S atoms at a longer distance outside the co-

Table 5. Crystal structure of marrucciite: Site occupancy factors (s.o.f.), atomic coordinates and equivalent isotropic displacement parameters U(eq/iso) (Å$^2$ × 10$^3$).

| Atom | s.o.f | x | y | z | U(eq/iso) x 10$^3$ | Atom | s.o.f | x | y | z | U(eq/iso) x 10$^3$ |
|---|---|---|---|---|---|---|---|---|---|---|---|
| Hg1 | | 0 | 0 | 1/2 | 24.2(6) | S2 | | –0.0555(3) | 1/2 | 0.4805(5) | 14(2) |
| Hg2 | | –0.12993(6) | 1/2 | 0.56857(10) | 31.6(5) | S3 | | –0.0771(3) | 0 | 0.5801(6) | 22(3) |
| Pb1 | | –0.02600(5) | 1/2 | 0.61767(9) | 23.3(4) | S4 | | –0.1931(3) | 0 | 0.4880(6) | 24(3) |
| Pb2 | | 0.06881(5) | 1/2 | 0.65812(9) | 23.3(4) | S5 | 0.5 | 0.2167(3) | 0.555(5) | 0.3926(7) | 22(4) |
| Pb3 | | –0.18617(5) | 0 | 0.37752(10) | 25.0(4) | S6 | 0.5 | –0.1278(3) | 0.551(5) | 0.6701(7) | 25(4) |
| Pb4 | | 0.21497(5) | 1/2 | 0.26235(9) | 24.7(4) | S7 | | –0.1386(3) | 1/2 | 0.4629(6) | 19(2) |
| Pb5 | | 0.11942(4) | 1/2 | 0.85218(9) | 20.1(4) | S8 | | –0.2349(3) | 1/2 | 0.3455(6) | 20(2) |
| Pb6 | | 0.16059(5) | 1/2 | 0.05133(9) | 23.9(4) | S9 | | 0.1639(3) | 0 | 0.2487(5) | 16(2) |
| Pb7 | | 0.11078(4) | 1/2 | 0.16352(9) | 22.5(4) | S10 | 0.5 | 0.3560(3) | 0.049(5) | 0.3201(7) | 27(4) |
| Pb8 | 0.63(3) | –0.0545(2) | 1/2 | 0.7468(4) | 21(2) | S11 | 0.5 | 0.1832(4) | 0.554(6) | 0.8635(8) | 33(5) |
| Sb8 | 0.37(–) | –0.0458(5) | 1/2 | 0.7568(12) | 21(–) | S12 | 0.5 | 0.2255(3) | 0.564(4) | 0.0483(7) | 22(4) |
| Pb9 | 0.41(3) | 0.0342(5) | 0 | 0.8194(11) | 28(3) | S13 | | 0.2707(3) | 1/2 | 0.2305(6) | 23(3) |
| Sb9 | 0.59(–) | 0.0377(6) | 0 | 0.8090(14) | 28(–) | S14 | | 0.3913(3) | 1/2 | 0.2426(5) | 18(2) |
| Sb1 | 0.5 | –0.0960(1) | 0.0818(10) | 0.46646(19) | 20(1) | S15 | | 0.1532(3) | 0 | –0.0448(6) | 20(2) |
| Sb2 | | –0.23449(10) | 1/2 | 0.44876(19) | 29.5(8) | S16 | | 0.1996(3) | 0 | 0.1554(5) | 16(2) |
| Sb3 | | 0.17107(9) | 0 | 0.35666(15) | 24.1(7) | S17 | | 0.0479(3) | 1/2 | 0.7570(6) | 23(3) |
| Sb4 | | 0.33929(8) | 1/2 | 0.24036(16) | 22.5(7) | S18 | | 0.0010(3) | 1/2 | 0.8633(6) | 23(3) |
| Sb5 | | 0.20481(9) | 0 | –0.0425(2) | 32.2(9) | S19 | 0.5 | –0.0472(3) | 0.542(6) | –0.0456(6) | 20(4) |
| Sb6 | | 0.24964(8) | 0 | 0.15138(16) | 23.0(7) | S20 | 0.5 | 0.0910(3) | 0.534(7) | –0.0556(6) | 21(4) |
| Sb7 | 0.5 | 0.07073(10) | 0.044(6) | –0.0138(2) | 29(4) | S21 | | –0.0203(3) | 0 | 0.7225(6) | 23(3) |
| Sb10 | 0.5 | –0.02174(12) | 0.038(10) | 0.9141(2) | 36(6) | S22 | | –0.0711(3) | 0 | 0.8130(5) | 16(2) |
| S1 | | 0.0190(3) | 0 | 0.6107(5) | 15(2) | S23 | | 0.1198(3) | 0 | 0.0861(5) | 17(2) |

U(eq) is defined as one third of the trace of the orthogonalized Uij tensor.

Table 6. Anisotropic displacement parameters ($Å^2 \times 10^3$) for cations in the crystal structure of marrucciite.

| Atom | $U_{11}$ | $U_{22}$ | $U_{33}$ | $U_{23}$ | $U_{13}$ | $U_{12}$ |
|---|---|---|---|---|---|---|
| Hg1 | 0.0272(14) | 0.0279(15) | 0.0170(12) | 0 | 0.0103(11) | 0 |
| Hg2 | 0.0452(13) | 0.0353(12) | 0.0259(10) | 0 | 0.0265(10) | 0 |
| Pb1 | 0.0301(11) | 0.0222(10) | 0.0249(9) | 0 | 0.0190(9) | 0 |
| Pb2 | 0.0324(11) | 0.0142(9) | 0.0243(9) | 0 | 0.0144(8) | 0 |
| Pb3 | 0.0223(10) | 0.0232(10) | 0.0287(10) | 0 | 0.0118(8) | 0 |
| Pb4 | 0.0261(10) | 0.0192(9) | 0.0228(9) | 0 | 0.0071(8) | 0 |
| Pb5 | 0.024(1) | 0.0168(9) | 0.0216(9) | 0 | 0.0126(8) | 0 |
| Pb6 | 0.0372(12) | 0.0159(9) | 0.0247(9) | 0 | 0.0198(9) | 0 |
| Pb7 | 0.023(1) | 0.0208(10) | 0.0294(10) | 0 | 0.0171(8) | 0 |
| Pb8/Sb8 | 0.020(4) | 0.0226(14) | 0.028(3) | 0 | 0.016(3) | 0 |
| Pb9/Sb9 | 0.019(5) | 0.0335(19) | 0.047(7) | 0 | 0.028(2) | 0 |
| Sb1 | 0.0176(19) | 0.024(4) | 0.0175(18) | –0.0015(15) | 0.0086(16) | –0.0009(15) |
| Sb2 | 0.048(2) | 0.0184(17) | 0.042(2) | 0 | 0.038(2) | 0 |
| Sb3 | 0.040(2) | 0.0167(16) | 0.0168(15) | 0 | 0.0150(15) | 0 |
| Sb4 | 0.0250(17) | 0.0265(18) | 0.0218(16) | 0 | 0.0160(14) | 0 |
| Sb5 | 0.0187(17) | 0.0186(17) | 0.059(3) | 0 | 0.0184(17) | 0 |
| Sb6 | 0.0199(16) | 0.0306(19) | 0.0223(16) | 0 | 0.0133(14) | 0 |
| Sb7 | 0.0141(17) | 0.039(13) | 0.0269(19) | –0.001(3) | 0.0048(14) | 0.012(4) |
| Sb10 | 0.032(2) | 0.033(17) | 0.026(2) | 0.011(6) | 0.0009(17) | 0.003(3) |

Table 7. Hg-S distances, bond valences and S-Hg-S angles in marrucciite and rouxelite.

| **Rouxelite *** | | | | **Marrucciite** | | | | | | | |
|---|---|---|---|---|---|---|---|---|---|---|---|
| | d (Å) | B. V. | | | d (Å) | B. V. | | | d (Å) | B. V. | |
| Hg-S3 × 2 | 2.381 | 0.85 | × 2 | Hg1-S1 × 2 | 2.361(11) | 0.90 | × 2 | Hg2-S7 | 2.369(12) | 0.88 | |
| -S2 × 4 | 3.267 | 0.08 | × 4 | -S2 × 4 | 3.230(11) | 0.09 | × 4 | -S6 | 2.404(15) | 0.80 | |
| Bond Valence Sum BVS | | 2.02 | | | BVS | 2.16 | | -S3 × 2 | 3.186(10) | 0.10 | × 2 |
| | | | | | | | | -S4 × 2 | 3.406(11) | 0.05 | × 2 |
| | | | | | | | | | BVS | 1.98 | |
| | | | | | Angles** | | | | | | |
| S2-Hg-S3 | 82.04° | | | S1-Hg1-S2 | 82.02° | | | S3-Hg2-S4 | 96.87° | | |
| « | 97.96° | | | « | 97.98° | | | S3-Hg2-S6 | 109.16° | | |
| S2-Hg-S2 | 76.82° | | | S2-Hg1-S2 | 80.85° | | | « | 102.44° | | |
| « | 103.10° | | | « | 99.15° | | | S4-Hg2-S6 | 102.61° | | |
| | | | | S3-Hg2-S7 | 79.22° | | | « | 96.48° | | |
| | | | | S4-Hg2-S7 | 75.13° | | | S6-Hg-S7 | 171.60° | | |
| | | | | S3-Hg2-S3 | 80.51° | | | S3-Hg-S4 | 154.23° | | |

B.V.: Bond valences calculated according to Brese & O'Keeffe (1991). * Orlandi *et al.* (2005).
** Angles equal to 180° are not indicated.

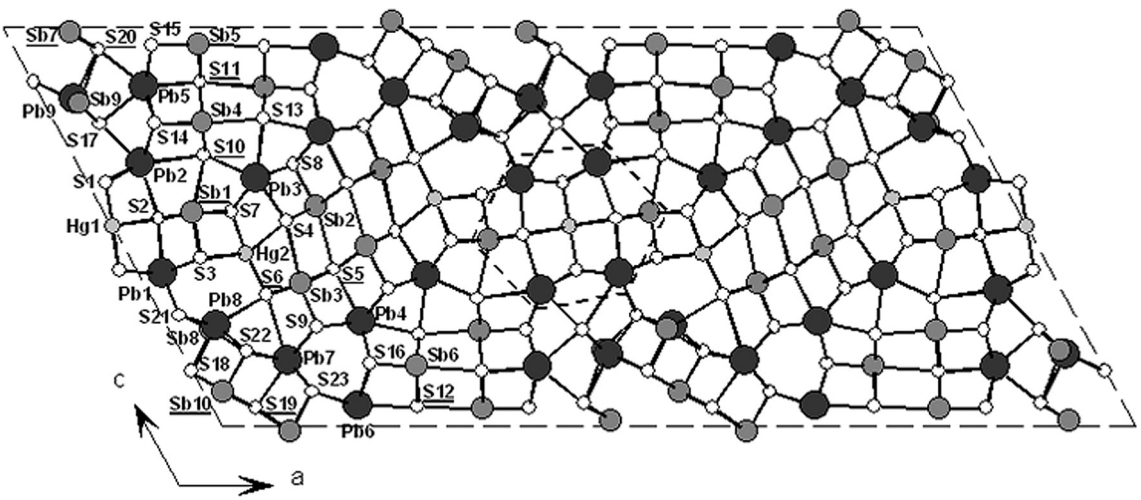


Fig. 3. Projection along *b* of the crystal structure of marrucciite (unit cell). In order of decreasing size: Pb (black), Sb (dark grey), Hg (light grey) and S (white). Sb and S atom labels corresponding to split positions along *b* are underlined. The central column $HgPb_4Sb_2S_4$ has been outlined.

Table 8. Pb-S distances, Pb bond valences and coordination types in marrucciite.

| | d (Å) | B. V. | | d (Å) | B. V. | | d (Å) | B. V. |
|---|---|---|---|---|---|---|---|---|
| Pb(1)-S(1) × 2 | 3.057(8) | 0.25 × 2 | Pb(2)-S(1) × 2 | 2.947(8) | 0.34 × 2 | Pb(3)-S(7) × 2 | 3.031(9) | 0.27 × 2 |
| -S(3) × 2 | 3.001(9) | 0.30 × 2 | -S(14) × 2 | 3.035(9) | 0.27 × 2 | -S(8) × 2 | 2.937(9) | 0.35 × 2 |
| -S(21) × 2 | 3.163(10) | 0.19 × 2 | -S(2) | 3.077(11) | 0.24 | -S(4) | 2.835(9) | 0.46 |
| -S(2) | 2.894(11) | 0.39 | -S(10) | 3.417(15) | 0.10 | -S(10) | 3.496(18) | 0.08 |
| -S(17) | 3.527(13) | 0.07 | -S(17) | 3.000(13) | 0.30 | -S(13) | 3.122(13) | 0.21 |
| *Type: 8s** | BVS | 1.94 | *Type: 7l* | BVS | 1.86 | *Type: 7l* | BVS | 1.99 |
| Pb(4)-S(8) × 2 | 3.071(9) | 0.25 × 2 | Pb(5)-S(14) × 2 | 2.926(8) | 0.36 × 2 | Pb(6)-S(15) × 2 | 2.986(9) | 0.31 × 2 |
| -S(9) × 2 | 3.108(9) | 0.22 × 2 | -S(15) × 2 | 3.023(9) | 0.28 × 2 | -S(16) × 2 | 3.083(8) | 0.24 × 2 |
| -S(16) × 2 | 3.093(8) | 0.23 × 2 | -S(11) | 2.968(17) | 0.32 | -S(23) × 2 | 3.227(9) | 0.16 × 2 |
| -S(5) | 3.103(14) | 0.22 | -S(17) | 3.090(13) | 0.23 | -S(12) | 3.183(15) | 0.18 |
| -S(13) | 3.135(13) | 0.21 | -S(20) | 3.125(13) | 0.21 | -S(20) | 3.098(13) | 0.23 |
| *Type: 8s* | BVS | 1.83 | *Type: 7l* | BVS | 2.04 | *Type: 8s* | BVS | 1.83 |
| Pb(7)-S(9) × 2 | 3.154(9) | 0.20 × 2 | | | | | | |
| -S(22) × 2 | 3.046(8) | 0.26 × 2 | | | | | | |
| -S(23) × 2 | 2.946(8) | 0.34 × 2 | | | | | | |
| -S(6) | 3.683(15) | 0.05 | | | | | | |
| -S(19) | 3.018(13) | 0.22 | | | | | | |
| *Type: 8s* | BVS | 1.87 | | | | | | |

*Nx**: *N* = coordination number (*7* or *8*)
*s* or *l* = orientation of the triangular prism (*s*: standing; *l*: lying)
BVS: Bond Valence Sum

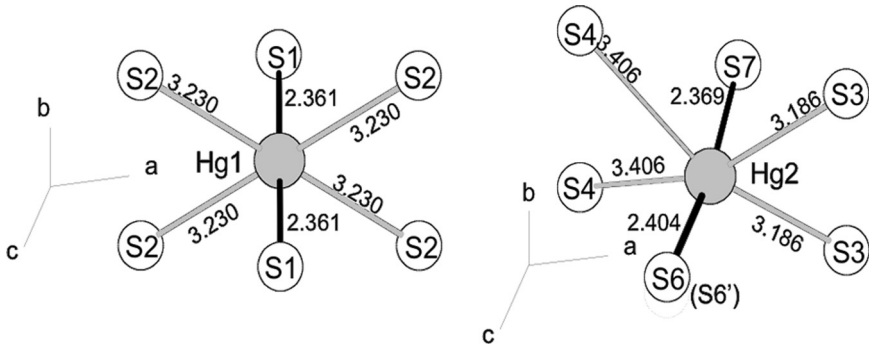


Fig. 4. Coordination of Hg atoms and Hg-S distances (Å) in the crystal structure of marrucciite.

rdination pyramid. Three Sb positions (Nos 1, 7 and 10) are split along *b*, with a statistical occupancy (50 %); they correspond to the Sb atoms with 5 + 2 coordination.

Mixed (Pb, Sb) sites: 2 sites (Nos 8 and 9) present a (Pb, Sb) pair with Pb and Sb on distinct positions. Site No 8 has major Pb with prismatic coordination (7*l*), while site No 9 has major Sb with (5 + 2) coordination.

S atoms: Their coordination will not be detailed. It should be noted that for 7 among the 23 positions the refinement indicated that they ought to be split along *b*.

## Split atom positions and superstructure

The splitting along *b* of several Sb and S atom positions is directly related to the 2*b* superstructure of marrucciite. Such a ~ 8 Å superstructure has been also observed for scainiite, pillaite, pellouxite and rouxelite (Orlandi, 1999; 2001; 2004; 2005), and is the consequence of an asymmetric trapezoidal coordination of Sb atoms, as pointed first by Makovicky & Mumme (1983) for the crystal structure of ramdohrite, $Pb_6Sb_{11}Ag_3S_{24}$. Such a pyramidal coordination with a trapezoidal basis favours the shortening of two Sb-S bonds towards one side of the trapeze, and creates a short-range ordering of Sb sites along the elongation (*i.e.* 4 Å) direction; it is a primary cause of a superstructure. For instance, a $n = 6$ superstructure was solved for andorite VI (or senandorite – $PbAgSb_3S_6$) by Sawada *et al.* (1987), but the most complex example up to now is given by the ninefold superstructure of the Pb-As sulfosalt sartorite (Berlepsch *et al.*, 2003).

In marruccite, as well as in related sulfosalts, every non-split Sb position thus corresponds to an average of at least two distinct positions, while a split Sb position (up and down along the elongation parameter) reveals its trapezoidal coordination. Splitting of adjacent S positions reinforces this interpretation, which indicates that all four 1D modules of marrucciite present this trapezoidal character. Nevertheless, attempts to split a greater number of Sb and S positions for marrucciite were unsuccessful. Even in the case of scainiite, where a ~ 8 Å superstructure could be registered (Moëlo *et al.*, 2000), the "splitting" (relatively to a ~ 4 Å structure) of all Sb positions did not permit to propose an ordered trapezoidal arrangement of Sb and S atoms.

## General architecture of the crystal structure

The crystal structure of marrucciite can be easily described according to the general principles of modular analysis developed by Makovicky (1981; 1985a) for lead sulfosalts and related compounds. Figure 5 delimitates a large pseudo-hexagonal motif organized around the central file of Hg1 atoms that will facilitate the modular description of the structure, as well as the comparison with other complex structures of the sulfosalt type. Figure 6 (left) is focused on the central part of this motif.

### *1D modules*

Figure 7 represents the four 1D building blocks at the root of the pseudo-hexagonal configuration in Fig. 6. The central column has the composition $HgPb_4Sb_2S_4$; it is a distorted derivative of PbS archetype, three-atom thick and two octahedra large. It is surrounded with a sub-hexagonal crown of 12 S atoms from the six neighboring rods. These six rods belong to three types (A, B and C), of the general formula $Me_{10}S_{14}$. These rods are four-atom thick, and three (hemi-)octahedra large, but each type has distinct chemical and geometrical features:

- rod A contains the second Hg position (Hg2). It is also a derivative of PbS archetype, with a strong dissymmetry of the octahedral coordination of Sb atoms, and a moderate SnS-type distortion (the rod elongation corresponding to the $b_{SnS}$ direction – del Bucchia *et al.*, 1981; Makovicky, 1985a);
- rod B contains exclusively Sb in the two inner atom slabs, and Pb exclusively at the margin. It is also derived from PbS archetype, with a strong octahedral dissymmetry, but without significant SnS-type distortion;
- rod C includes the two (Pb, Sb) mixed sites. It is clearly of the SnS archetype, with $c_{SnS}$ as its elongation direction. Within each rod, Sb atoms delimitate lone electron pair micelles (ellipses in Fig. 5).

### *2D module connection*

Arrows in Fig. 7 indicate the interconnection between the three types of rods and the central column, *via* the crown of 12 S atoms around it. Each rod is symmetrically connected

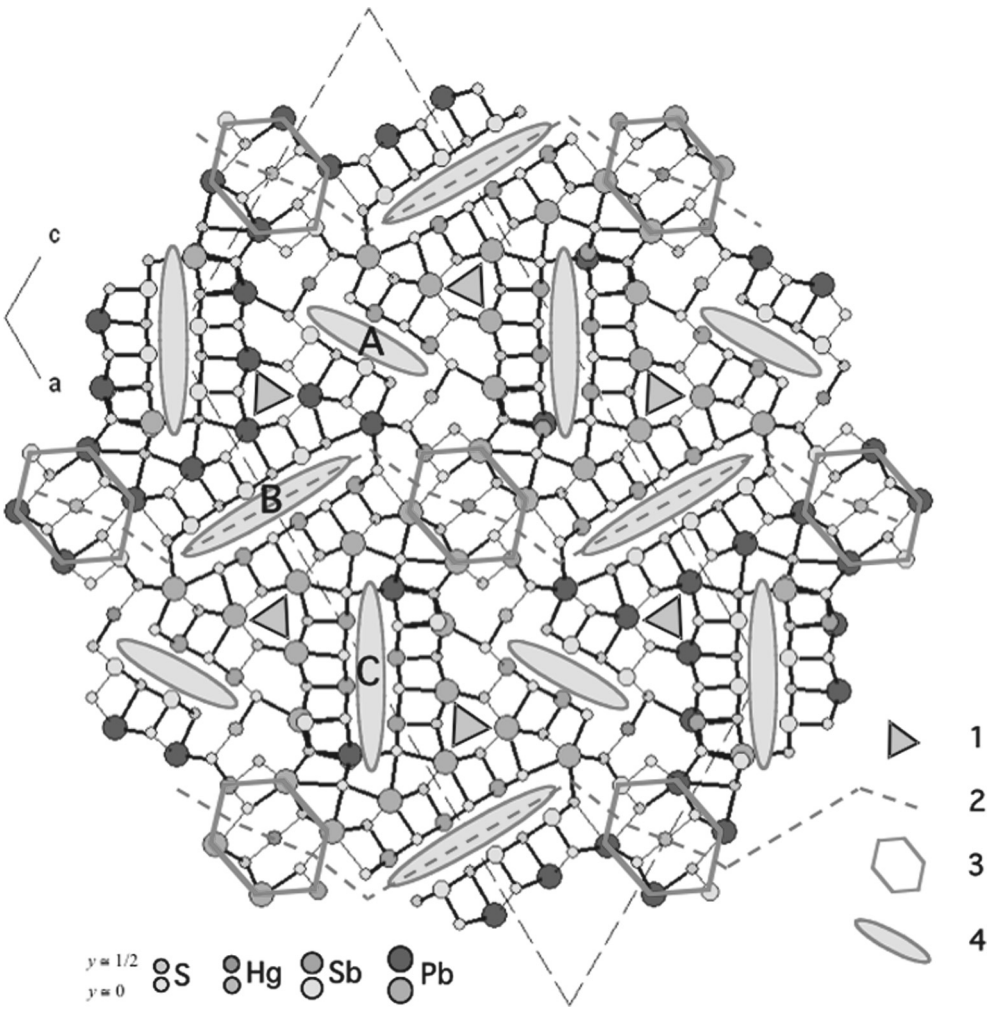


Fig. 5. Enlarged projection of the crystal structure of marrucciite showing its pseudo-hexagonal architecture. The darkest and lightest tints of each atom type correspond to *y* close to ½ and 0, respectively. 1. Local pseudo-trigonal axis; 2. Limit of complex „rod-layer" (M of Fig. 9); 3. Central column; 4. Interspace (micelles) where Sb lone electron pairs are pointing.

to another central column (Fig. 5), giving the whole structure. Two other important crystallographic aspects must be pointed out:

(1) Three rods (one of each type) interconnect around a pseudo-trigonal axis (triangles of Fig. 5) formed by three lead atoms (Pb Nos 4, 6 and 7) with a standing bicapped trigonal prismatic coordination. Such a pseudo-trigonal local configuration is characteristic of sulfosalts of the zinkenite family (Makovicky, 1985b); here it points directly to the crystal structure of hexagonal $Ba_{12}Bi_{24}S_{48}$ (Aurivillius, 1983).

(2) Hg-bearing building blocks (the central column plus the two adjacent rods of type A) are interconnected *via* short Sb-S and Hg-S bonds to constitute a "rod-layer" parallel to (001) (M in Fig. 8).

## Structural relationships with other sulfosalts

### Marrucciite and $Ba_{12}Bi_{24}S_{48}$

As indicated above, the crystal structure of marrucciite is closely derived from that of hexagonal $Ba_{12}Bi_{24}S_{48}$ (Aurivillius, 1983). Relatively to this hexagonal archetype (Fig. 6 right), marrucciite differs essentially (Fig. 6 left):

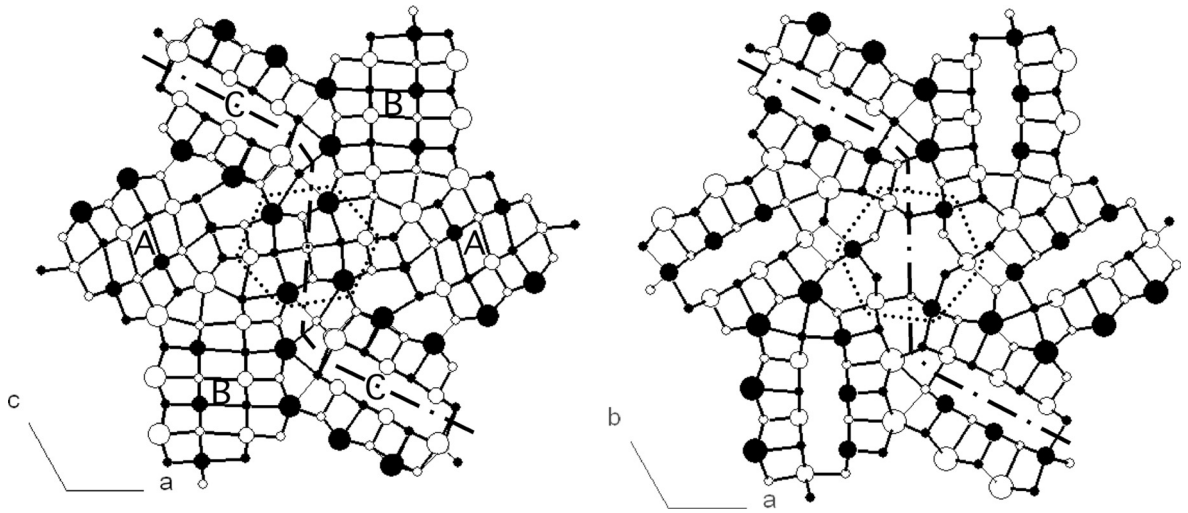


Fig. 6. Comparison between the pseudo-hexagonal motif of marruccite (left – one central column (outlined) with its crown of the six A, B and C rods) and the hexagonal one of $Ba_{12}Bi_{24}S_{48}$ (right – the central channel with atom wall $Bi_6S_6$ has been outlined). The tie-line separates each motif in two symmetric parts (see text).

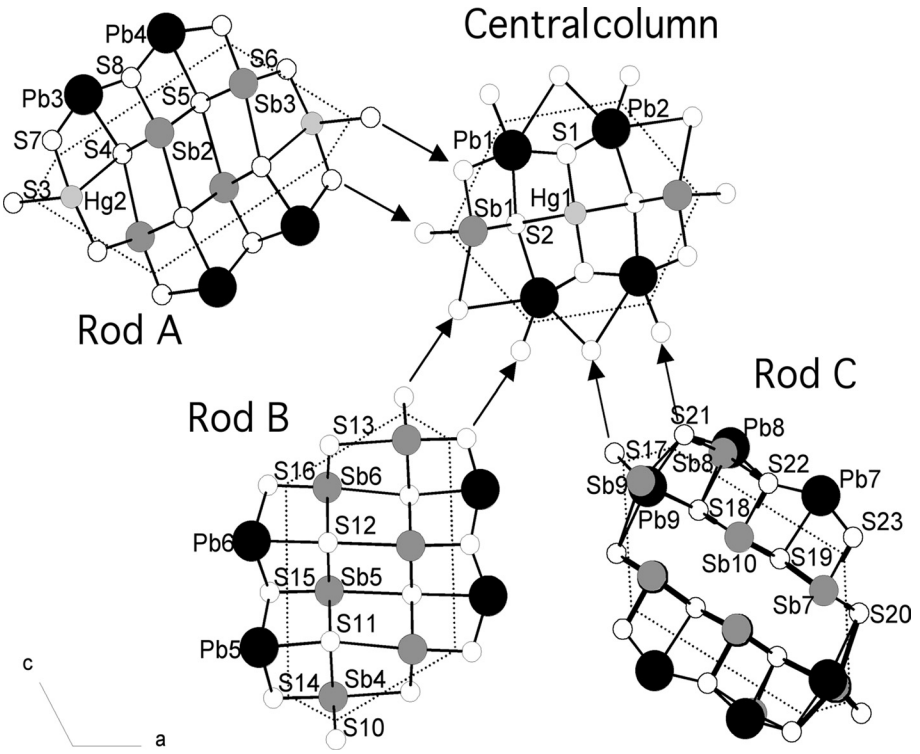


Fig. 7. Interconnection between the central column and the three other constitutive rods A, B and C of the crystal structure of marrucciite.

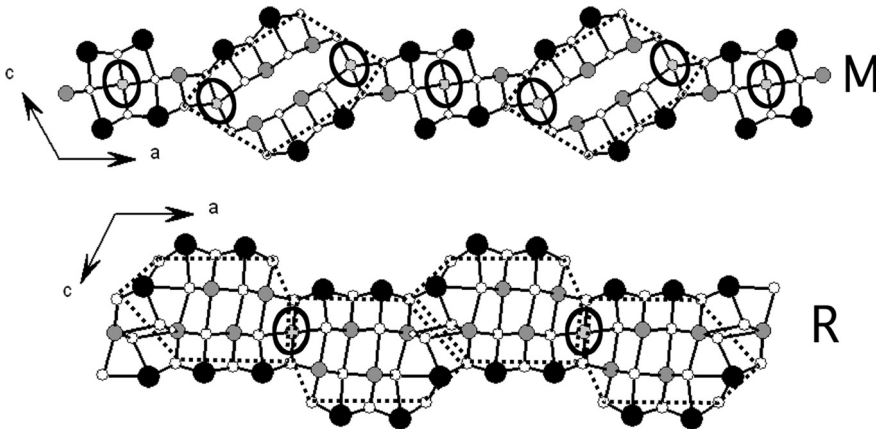


Fig. 8. Combination of the Hg bearing rod and column forming the specific rod-layer of marrucciite structure (M). Comparison with the Hg bearing rod-layer of rouxelite (R). Hg atoms are located within the ellipses; A-type rods in M layer and truncated derivatives in R layer are visualized by doted lines.

(1) by the replacement of the central column $Bi_6S_6$ around the empty hexagonal axis by a Hg-filled pseudo-orthorhombic one, $HgPb_4Sb_2S_4$;

(2) by the SnS-type organization of the C rod of marrucite, due to the (5+2) asymmetric coordination of Sb (strong stereochemical activity of the lone electron pair), while in $Ba_{12}Bi_{24}S_{48}$, all Bi atoms present a distorted octahedral coordination. As a result, the two C rods break down the hexagonal periodicity around the central column, as indicated by the zigzag tie-lines: the right part of the marrucciite motif is 3D-topologically identical to the right part of $Ba_{12}Bi_{24}S_{48}$ motif, while in the left part all atoms are shifted by $\Delta y = ½$ against the right part.

In 2D projection along the elongation axis, from a topologic point of view (*i.e.* disregarding the $\Delta y \sim ½$ shift), 80 [010] atom rows of maruccite crystal structure (24×3 from A-B-C rods + 8 from the central column – 4 Pb, 2 Sb, 2S) have their equivalent among the 84 [001] atom rows of the structure of $Ba_{12}Bi_{24}S_{48}$, while only the central Hg1 position and two S atoms are specific in marrucciite. This gives a two-dimensional topologic similarity index of ~ 95 % for marrucciite structure relatively to that of parent $Ba_{12}Bi_{24}S_{48}$.

## Marrucciite and scainiite

Like that of marrucciite, the crystal structure of scainiite is a monoclinic derivative of hexagonal $Ba_{12}Bi_{24}S_{48}$, by means of a more complex derivation scheme, which implies a 1D expansion of the original structure, through the intercalation of a kermesite type ribbon (Moëlo *et al.*, 2000). This explains a lower 2D-topological similarity index of 82 % for the scainiite structure relatively to that of $Ba_{12}Bi_{24}S_{48}$.

The direct comparison between marrucciite and scainiite crystal structures is visualized in Fig. 9, considering complex "palissadic" layers (*i.e.* thick layers formed by the connection of complex columns). In this figure, the complex layer (M) of marrucciite is a 2D structure fragment limited by the surfaces of weakest bonding, along the median planes of lone electron pair micelles, as applied initially to the structure of scainiite (S – Moëlo *et al.*, 2000). Among the three possibilities due to the pseudo-hexagonal symmetry of marrucciite (Fig. 5), the layer parallel to $(20\bar{1})$ appears as the most favourable, giving a "palissadic" layer (M in Fig. 9) where each constitutive column is formed by two symmetric fragments with pseudo-trigonal symmetry. Moreover, surfaces defined in this way may correspond to the observed cleavage plane.

The equivalent palissadic layer in the crystal structure of scainiite (S in Fig. 9) presents a stretching of the connection between two successive pairs of triangular rods, due to the intercalation of a kermesite-type ribbon. The second difference is that, at the layer margin, the Hg1 position (half-shared with the neighbouring rod-layer) of marrucite corresponds to the $SbSO_{0.5}$ group in scainiite. The rests of the two structures, corresponding to 82 positions (atom rows) in a 2D projection, are topologically identical.

In the two structures, the periodicities along the palissadic layers on the one hand, and, on the other hand, in the stacking direction, correspond to [102] and $[10\bar{2}]$ respectively. One has thus:

- close stacking $[10\bar{2}]$ periodicities, 83.02 Å (marrucciite) against 79.36 Å (scainiite);
- angles between [102] and $[10\bar{2}]$ close to 90° (90.28° and 93.96°, respectively);
- a higher periodicity along [102] for scainiite (61.94 Å) than for marrucite (49.06 Å).

## Hg environment in marrucciite and other Hg sulfosalts

Up to now, adding this new sulfosalt, there are 16 sulfosalts with Hg as a specific constituent (Strunz & Nickel, 2001; Orlandi *et al.*, 2005). Among the known crystal structures within this group, only that of rouxelite, recently defined at Buca della Vena (Orlandi *et al.*, 2005), presents some similarities regarding the local Hg environment, as illustrated by the two Hg bearing layers M and R of Fig. 8. While in marrucciite (M) one has the alternation of the A rod with the central column, in rouxelite (R) there is only one type of rod, corresponding to a truncated derivative of A rod, with formula $Hg_{0.5}Pb_5Sb_4S_{10}(O,S)_{0.5}$. This configuration yields the

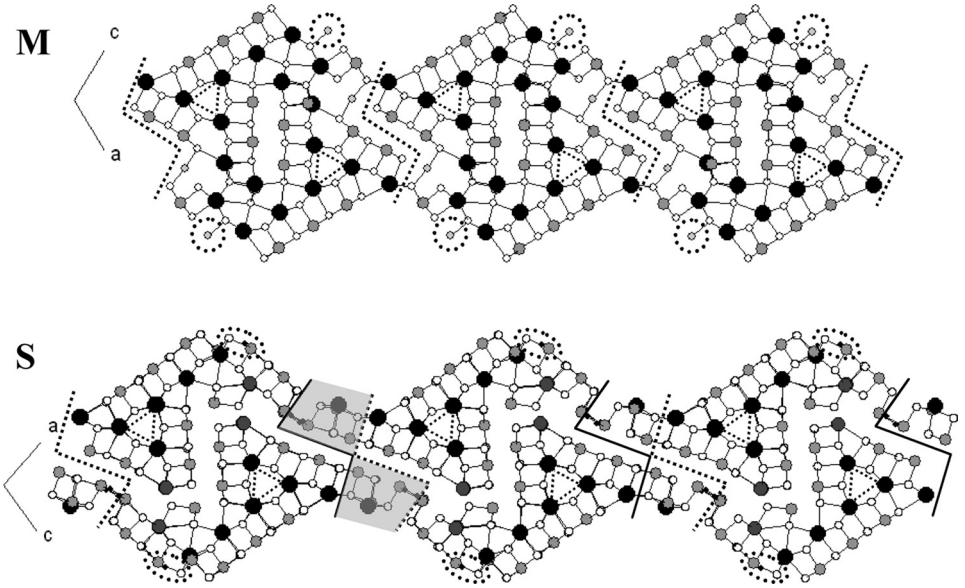


Fig. 9. Marrucciite structure (*M*): Cut-off along surfaces of weakest bonding, delimiting a palissadic layer parallel (20$\bar{1}$). Dotted lines separate adjacent complex columns, formed by two fragments organized around pseudo-trigonal axes (doted triangles). *S*: Equivalent palissadic layer of scainiite (Moëlo *et al.*, 2000). Grey area in scainiite represents the intercalated kermesite-type ribbon. Other crystal chemical differences at the margin are marked by doted circles (*M*: half a Hg atom) and ellipses (*S*: $SbSO_{0.5}$).

composition $Hg_2Pb_4Sb_4S_{14}$ + $HgPb_4Sb_2S_4$ = $Hg_3Pb_8Sb_6S_{18}$ in marrucciite, whereas the alternation of two symmetric truncated rods gives the total of $HgPb_{10}Sb_8S_{20}(O,S)$ in rouxelite.

## Conclusions

Marrucciite is a new complex Hg bearing sulfosalt, the third defined in the Apuan Alps after grumiplucite, $HgBi_2S_4$ (Orlandi *et al.*, 1998), and rouxelite, $Cu_2HgPb_{22}Sb_{28}S_{64}(O,S)_2$ (Orlandi *et al.*, 2005), and 16$^{th}$ among all known Hg sulfosalts (Strunz & Nickel, 2001; Orlandi *et al.*, 2005). Its conditions of formation at Buca della Vena are identical to those proposed for rouxelite, that is the hydrothermal remobilisation and deposition of mercury in Apuane Alps through the Apenninic tectono-metamorphic event, in low temperature conditions (Dini *et al.*, 2001; Orlandi *et al.*, 2005).

According to modular analysis, the crystal structures of marrucciite, scainiite and pellouxite (Palvadeau *et al.*, 2004) correspond to SnS-type monoclinic derivatives of primitive hexagonal $Ba_{12}Bi_{24}S_{48}$; they belong to the same architectural family of plesiotypic compounds (Makovicky,1997; Ferraris *et al.*, 2004), within the larger group of so-called cyclically organized sulfosalt structures and related compounds (Makovicky, 1985b).

In each of these three structures, specific chemical elements with minor contents (~ 4–5 at. %) play a critical role for their formation: Hg in marrucciite (3 at. among a total of 83 at. in the structural formula), O in scainiite (5 among 103 at.), O, (Ag, Cu) and Cl in pellouxite (4 at. among 103 at.). This is also true for the two other new Pb-Sb sulfosalts from Buca della Vena: pillaite (O and Cl – 3 at. among 87) and rouxelite (Cu, Hg and O – about 4 at. among 119). Therefore, the fundamental question is: "how such minor components control the formation and stabilization of such complex compounds, thus permitting an energy benefit ?" Today, there is no universal response to such diverse elements, but one important aspect is that each minor element has a key role for the stabilization of a specific 1D- or 2D module within a given structure.

## Addendum

by Ernst Burke, Chairman of the CNMNC of the IMA

E-mail: ernst.burke@falw.vu.nl

The first work on this Hg-Pb-sulphosalt from the Slovakian locality Gelnica was carried out in Amsterdam in 1969 in cooperation between Milan Háber and myself. We were not able to define a unit cell at that time. Synthetic material was made in Bratislava and studied in Moscow in the 1970s. Data were published (without a name for the mineral) by Háber & Babčan (1971) and with the names 'gelnicite' by Háber (1980) and Háber *et al.* (1999), and finally with the name 'gelnicaite' by Háber *et al.* (2004). The name 'gelnicite' was also used in the book by Papp (2004). I have repeatedly told Milan Háber, in the 1970s and in 2004, that approval of the CNMMN should be asked to use the names for the Slovak mineral, but apparently to no avail. The inclusion of my name as author in the 2004 publication happened without my prior knowledge, and certainly without my approval.

**Acknowledgements:** This study has been performed with the contribution of CNR, Istituto di Geoscenze e Georisorse del CNR di Pisa. Critical comments and suggestions by Dr. I. Baksheev (Moscow State University) as well as an anonymous reviewer were greatly appreciated. We thank O. Rouer (CNRS Orléans) for his help in microprobe analysis.

## References


Aurivillius, B. (1983): The crystal structure of two forms of $BaBi_2S_4$. *Acta Chem. Scand.*, **A37**, 399–407.

Benvenuti, M., Lattanzi, P., Tanelli, G., Cortecci, G. (1986): The Ba-Fe-pyrite deposit of Buca della Vena, Apuan Alps, Italy. *Rend. Soc. Ital. Mineral. Petr.*, **41**, 347–358.

Berlepsch, P., Armbruster, T., Makovicky, E., Topa, D. (2003): Another step toward understanding the true nature of sartorite: Determination and refinement of a ninefold superstructure. *Am. Mineral.*, **88**, 450–461.

Brese, N. E. & O'Keeffe, M. (1991): Bond-valence parameters for solids. *Acta Crystallogr,* B**47**, 192–197.

Criddle, A.J. & Stanley, C.J. (1993): Quantitative data file for ore minerals (QDF3, COM-IMA). Chapman & Hall ed., London, 700 p.

del Bucchia, S., Jumas, J.C., Maurin, M. (1981): Contribution à l'étude de composés sulfurés d'étain (II): Affinement de la structure de SnS. *Acta Crystallogr,* B**37**, 1903–1905.

Dini, A., Benvenuti, M., Costagliola, P., Lattanzi, P. (2001): Mercury deposits in metamorphic settings: the example of Levigliani and Ripa mines, Apuane Alps (Tuscany, Italy). *Ore Geol. Rev.*, **18**, 149–167.

Ferraris, G., Makovicky, E., Merlino, S. (2004): Crystallography of modular materials. Oxford University Press, 370 p.

Háber, M. (1980): Mineralogisch-geochemische und paragenetische Erforschung hydrothermaler Gänge im Gebiet zwischen Prakovce und Kojšov (Spišsko-gemerské rudohorie). *Západné Karp. Mineral., Petrogr., Geochém., Metalog.*, **7**, 7–131 (in German).

Háber, M. & Babčan, J. (1971): Preliminary identification of $5PbS.HgS.Sb_2S_3$ sulphosalt and attempt of its synthesis. *Mineralia Slovaca*, **3**, 261–261 (in Slovak).

Háber, M., Jelen, S, Krizáni, I, Soták, J., Spisiak, J. (1999): Exkurzný sprievodca II, Banská Bystrica 21.–22. mája 1999 (in Slovak).

Háber, M., Babcan, J., Burke, E.A.J., Simonov, M.A., Ozdin, D. (2004): Gelnicait – Nova sulfosol (?) z locality Zenderling pri Gelnici. *Natura Carpatica*, **XLV**, 229–230 (in Slovak); *Mineralogical Abstracts*, 05M/3578.

Makovicky, E. (1981): The building principles and classification of bismuth-lead sulphosalts and related compounds. *Fortschr. Mineral.*, **59**, 137–190.

– (1985a): The building principles and classification of sulphosalts based on the SnS archetype. *Fortschr. Mineral.*, **63**, 45–89.

– (1985b): Cyclically twinned sulphosalt structures and their approximate analogues. *Z. Kristallogr.*, **173**, 1–23.

– (1997): Modular crystal chemistry of sulphosalts and other complex sulphides. *in* "Modular aspects of Minerals", Merlino S., ed. *EMU Notes in Mineralogy*, Vol. 1, Chap. 3, 237–271.

Makovicky, E. & Mumme, W.G. (1983): The crystal structure of ramdohrite, $Pb_6Sb_{11}Ag_3S_{24}$, and its implications for the andorite group and zinckenite. *N. Jb. Mineral. Abh.* **147**, 58–79.

Moëlo, Y., Meerschaut, A., Orlandi, P., Palvadeau, P. (2000): Lead-antimony sulfosalts from Tuscany (Italy): II – Crystal structure of scainiite, $Pb_{14}Sb_{30}S_{54}O_5$, an expanded monoclinic derivative of $Ba_{12}Bi_{24}S_{48}$ hexagonal sub-type (zinkenite series). *Eur. J. Mineral.*, **12**, 835–846.

Orlandi, P. & Checchi, F. (1986): The Buca della Vena mine, Tuscany, Italy. *Mineral. Rec.*, **17**, 261–268.

Orlandi, P. & Dini, A. (2004): Die Mineralien der Buca della Vena-mine, Apuaner Berge, Toskana (Italien). *Lapis*, **29**, 11–24.

Orlandi, P., Dini, A., Olmi, F. (1998): Grumiplucite, a new mercury-bismuth sulfosalt species from the Levigliani mine, Apuan Alps, Tuscany, Italy. *Can. Mineral.*, **36**, 1321–1326.

Orlandi, P., Moëlo, Y., Meerschaut, A., Palvadeau, P. (1999): Lead-antimony sulfosalts from Tuscany (Italy): I – Scainiite, $Pb_{14}Sb_{30}S_{54}O_5$, the first Pb-Sb oxy-sulfosalt, from Buca della Vena mine. *Eur. J. Mineral.*, **11**, 949–954.

Orlandi, P., Moëlo, Y., Meerschaut, A., Palvadeau, P. (2001): Lead-antimony sulfosalts from Tuscany (Italy). III. Pillaite, $Pb_9Sb_{10}S_{23}ClO_{0.5}$, a new Pb-Sb chloro-sulfosalt, from Buca della Vena mine. *Eur. J. Mineral.*, **13**, 605–610.

Orlandi, P., Moëlo, Y, Meerschaut, A., Palvadeau, P., Léone, P. (2004): Lead-antimony sulfosalts from Tuscany (Italy). VI. Pellouxite, ~$(Cu,Ag)_2Pb_{21}Sb_{23}S_{55}ClO$, a new oxy-chloro-sulfosalt, from Buca della Vena mine, Apuan Alps. *Eur. J. Mineral.*, **16**, 839–844.

Orlandi, P., Meerschaut, A., Moëlo, Y., Palvadeau, P., Léone, P. (2005): Lead-antimony sulfosalts from Tuscany (Italy). VIII. Rouxelite, $Cu_2HgPb_{22}Sb_{28}S_{64}(O,S)_2$, a new sulfosalt from Buca della Vena mine, Apuan Alps: Definition and crystal structure. *Can. Mineral.*, **43**, 919–933.

Palvadeau, P., Meerschaut, A., Orlandi, P., Moëlo, Y. (2004): Lead-antimony sulfosalts from Tuscany (Italy). VII. Crystal structure of pellouxite, ~$(Cu,Ag)_2Pb_{21}Sb_{23}S_{55}ClO$, an expanded monoclinic derivative of $Ba_{12}Bi_{24}S_{48}$ hexagonal sub-type (zinkenite group). *Eur. J. Mineral.*, **16**, 845–855.

Papp, G. (2004): History of minerals, rocks and fossil resins discovered in the Carpathian Region. *Studia Naturalia*, **15**, 215 p.

Sawada, H., Kawada, I., Hellner, E., Tokonami, M. (1987): The crystal structure of senandorite (andorite VI): $PbAgSb_3S_6$. *Zeit. Kristallogr.* **180**, 141–150.

Strunz, H. & Nickel, E.H. (2001): Strunz Mineralogical Tables. Chemical-structural mineral classification system (9th ed.). E. Schweizerbart'sche Verlagsbuchhandlung, Stuttgart, 870 p.


*Received 25 September 2006*
*Modified version received 29 November 2006*
*Accepted 24 January 2007*